Microstructures of binary Cr–xNi alloys ($0 \leq Ni \leq 50$ wt.%) in their as-cast state and after high temperature exposure

Elodie Conrath, Patrice Berthod

Microstructures of binary Cr-xNi alloys (0 ≤ Ni ≤ 50wt.%) in their as–cast state and after high temperature exposure

Elodie Conrath*, Patrice Berthod
Institut Jean Lamour, Department N°2: Chemistry and Physic of Solids and Surfaces
Team "Surface and interface, chemical reactivity of materials"
Faculty of Sciences and Techniques, Nancy – University,
B.P. 70239, 54506 Vandœuvre-lès-Nancy – France
*Corresponding author, email elodie.conrath@univ-lorraine.fr

Authors' emails elodie.conrath@univ-lorraine.fr and pberthodcentralelille1987@orange.fr

Post-print version of the article Materials at High Temperatures (2018) 33(2) 189–197.
DOI 10.1080/09603409.2016.1144317

Abstract: Metallic materials designed for uses at very high temperature must be based on elements with high melting points. In this work, several binary alloys, chosen in the Cr-rich part of the Cr-Ni diagram, were elaborated by foundry and characterized by metallography in the as-cast condition and after exposure at 1200°C. Many of the obtained alloys are composed of imbricated BCC chromium phase saturated in Ni and FCC nickel phase saturated in Cr. These structures may evolve more or less at high temperature. High values of hardness were obtained for some of these alloys, suggesting high strength at elevated temperature. The hardness evolution versus the Cr content was well represented by a law of mixture of the volume fractions and the hardness of the separated phases. Already intrinsically resistant against oxidation at high temperature, most alloys are also not sensitive to internal nitridation, contrarily to pure Cr. Such Cr-Ni alloys may be considered as possible bases for heat resistant alloys.

Keywords: Cast Cr-Ni alloys; High temperature; Aging treatment; Microstructures; Hardness; Internal nitridation

1. Introduction

With more and more extreme application conditions for the components working at elevated temperatures, there is a huge need of materials resistant to high mechanical loading. In order to have a good behaviour against cracks propagation, proper toughness is necessary and thus ceramic materials must be avoided because of their brittleness. Using highly refractory metallic materials is compulsory. In this field, numerous studies were devoted to alloys based on nickel, cobalt or iron. Indeed, these elements are the bases of a lot of refractory alloys and superalloys [1, 2]. The bests of these alloys are either based on nickel, single-crystalline and strengthened by γ /γ' particles, or based on cobalt and strengthened by carbides very stable at high temperature.

These superalloys always contain high chromium contents, generally between 20 and 30 wt.%, bringing them a good resistance to oxidation, thanks to the formation of a chromia protective scale [3]. This chromia scale is effective to protect the alloys against oxidation by hot gases in aero-engines (as alumina), but also against corrosion by molten substances (as CMAS). But the use of these superalloys is limited by their low mechanical strength at high temperature (about 1000°C for the Co-based ones and 1100°C for the Ni-based ones).

Chromium has a high temperature of fusion (according to different references: 1875°C [4] or 1907°C [5]). The crystalline network of chromium is body-centered cubic (BCC) at all temperatures. This structure is not as compact as the face-centred cubic (FCC) one of the nickel-based or of nickel-stabilized cobalt-based alloys. Only a few studies were done concerning chromium-based alloys, notably the Ni-containing ones. This work was undertaken to explore this family of refractory alloys. It was notably focused on the microstructures of simple alloys in their as-casted condition and on their microstructure evolution during aging at high temperature. These binary alloys are candidate to constitute the basis of more complex and efficient alloys. Their main element is chromium and they contain 0 to 50 wt.% of nickel. Their as-cast compositions, their microstructures and hardness in the as-cast state and after exposure at 1200°C were investigated. The gathered knowledge will be useful for developing more complex alloys improved by the presence of additional elements and strengthening particles.

2. Experimental details

2.1 Elaboration of the alloys

Nine chromium-based alloys containing 0 to 50wt.% of nickel were synthesized by foundry by targeting the compositions presented in Table 1.

In each case, pure elements (Cr: Delachaux purity 99.7% and Ni: Eramet purity 99.97%) were melted together in a high frequency induction furnace (CELES, Figure 1). All steps (heating, melting, the 5 minutes liquid-state stage, solidification and cooling) were done inside the cold copper crucible of the CELES furnace. This crucible was located inside a closed silica tube which allowed heating and melting the alloys in an inert atmosphere made of pure argon (600mbar, Alfagaz 1). To avoid the presence of not molten particles of chromium (possible problem due to its high melting

temperature), all alloys were 'remelted' following the same temperature cycle as the first cycle. Nine compact ingots of 40 grams were obtained.

2.2 Metallographic preparation

These nine alloys were cut using a DELTA BUELHER saw in order to obtain samples of two types: one metallographic sample was used for the examination of the as-cast microstructure, and the second sample was shaped with the form of a parallelepiped and used to perform aging test (approximate dimensions: 8 mm × 8 mm × 2mm).

In order to allow metallographic examination, the as-cast samples and the aged samples were embedded in a cold resin mixture (resin CY230 + hardener HY956, ESCIL, FRANCE).

The embedded alloys were ground by using SiC-enriched papers with a range of roughness from 80 to 4000 grit. After cleaning using ultrasonic vibrations in ethanol, the metallographic samples were polished using a non-woven textile disk containing SiO_2 particles (OPS 0.4µm, Struers). Then, a mirror-like state was obtained for all the metallographic samples to allow their characterization using X-Ray Diffraction (XRD) and Scanning Electron Microscopy (SEM).

The parallelepiped samples used for the furnace aging tests were polished with SiC papers (from 80 to 1200 grit). All edges and corners were chamfered and smoothed using the same SiC paper.

2.3 Furnace aging

The aging experiments were realized in a furnace (under laboratory air) to induce possible microstructure evolutions and to observe them by metallography.

The thermal cycle was composed of a heating step at +20°C/min, an isothermal stage of 50h at 1200°C and a cooling step at -5°C/min. Cooling was slow enough to avoid any thermal shock. The aged alloys were thereafter cut and prepared for metallographic observations (procedure already described above).

2.4 Characterization

All the alloys in the as-cast state were characterized by X-Ray Diffraction (XRD), using a Philips X'Pert Pro diffractometer, to identify the different phases.

The alloys in the as-cast state condition, as well as after aging treatment, were characterized in cross-section by SEM (Scanning Electron Microscopy, JEOL JSM-6010LA). The micrographs were realized in the BEC mode (Backscattered Electron Composition image) or in the BES mode (Backscattered Electron Shadow image).

Quantitative analyses were performed by EDS analysis (Energy Dispersive Spectroscopy analysis) and X-Ray cartographies were realized.

With the aim of evaluating the surface percent of each phase for the alloys, the Photoshop software (Adobe Photoshop CS, 8.0.1 Version) was used on BEC micrographs taken in four random zones on each alloy at 1000-fold magnification.

To characterize the influence of the addition of nickel to chromium on the hardness of the alloys, indentation tests were performed for each alloy at ambient temperature, with a 5kg-load. Five indentations were done according to the Vickers method (so all results in HV_5) for all the alloys in the as-cast state and in the aged state (50 hours, 1200°C). An average value and standard deviation were calculated in all cases. Moreover, to understand the evolution of hardness, a law of mixture of the volume fractions and hardness of the separated phases was calculated.

3. Results

3.1 Chemical composition

The chemical compositions of the nine alloys were verified by SEM. Five full frame EDS measurements at a 250-fold magnification were performed to calculate the average and the standard deviation of the Cr and Ni contents of each alloy (Table 2).

Globally, the chemical compositions obtained for the eight Cr-Ni alloys well fit the ones which were initially wished. The standard deviation is small in each case (± 0.9wt.% maximum).

For the 100Cr alloy, five EDS measurements were carried out to verify that no impurities were present. Pure chromium without any impurity was confirmed.

3.2 As-cast microstructure of the alloys

Exemplarily as-cast microstructures of some of the nine alloys are presented in Figure 2, Figure 3 and Figure 4.

In the case of the Cr-50Ni alloy (Figure 2), the matrix is a Ni-based one. It contains about 52wt.% of Ni (grey colour) and represents about 86% percent of its surface fraction (Table 3).

This matrix is face-centered cubic (FCC), as revealed by XRD, in accordance with the binary Cr-Ni diagram shown in Figure 5. This diagram was calculated using the software Thermo-Calc [6] and the database SSOL (STGE) [7].

The interdendritic compound is composed of the same Ni-phase like the dendrites and of a body-centered cubic (BCC) Cr-phase (about 70wt.% of Cr) containing Ni. Its morphology is typical of a eutectic compound. This double-phased structure is in good agreement with the phase diagram of the Cr-Ni binary system (Figure 5).

For the alloys containing more chromium and less nickel e.g. Cr-40Ni and Cr-30Ni, the matrix has changed. It is composed of a dark grey chromium phase (Figure 3). XRD diffractograms showed that this phase is BCC. The chromium matrix contains some nickel: 35 wt.% for the Cr-40Ni alloy and 18wt.% for the Cr-30Ni alloy.

The second phase (pale grey colour) is based on nickel and it contains chromium: 50 to 70 wt.% of Cr (detected by EDS analysis), depending on the alloy. The Cr matrix is the first phase to solidify. At the same time, the segregation of nickel in the liquid during the cooling step permitted the solidification of the second phase at the grain boundaries and the interdendritic spaces.

In the case of the Cr-20Ni alloy (Figure 4 top), the diminution of the nickel content induced a diminution of the surface fraction of the nickel phase (35 to 40 wt.% nickel (white colour) inside the interdendritic spaces). In the Cr-10Ni alloy (Figure 4 bottom), this phase totally disappeared. A zone enriched in nickel is visible in pale grey colour (20wt.% of Ni) which corresponds to nickel in solid solution inside the periphery of the grains of chromium phase.

In the cases of the alloys containing more than 90wt.% of Cr (Cr-7.5Ni, Cr-5Ni, Cr-2.5Ni), only one phase is visible. These three alloys are composed of a chromium-based matrix, containing some nickel in solid solution. This is confirmed by the XRD results since only this BCC phase was detected.

The last sample, the pure Cr one, is logically single-phased and it is composed of pure chromium. No impurities were found by using XRD or SEM.

3.3 Evolution of the microstructures during high temperature exposure

A high temperature exposure of 50 hours at 1200°C induced structural coarsening for all the alloys containing nickel (Figures 6 to 9). Indeed, during the isothermal stage (at 1200°C, 50h), the alloys tried to reach the thermodynamic equilibrium corresponding to their composition and the aging temperature, but also to minimize their energy by optimizing morphology. The general trend of energy decrease led to a progressive diminution of the cumulative interface area between the Cr-phase and the Ni-phase. Furthermore, during the first part of the slow cooling (minus 5°C per minute), the alloys tended to reach successive equilibria.

In the specific case of the Cr-50Ni alloy, after the cooling from 1200°C to room temperature, the matrix is still composed of a nickel-based phase with a few chromium phases (in dark grey colour, cf. Figure 6). These chromium phases are coarser than in the as-cast state (Figure 2) and they represent about 9.9 surface percent (± 3.1%) of the alloy, which is almost the same quantity as in the as-cast Cr-50 alloy (Table 3).

In the case of the other alloys containing at least 60wt.% of chromium, the matrix is composed of a chromium phase (like in the as-cast state, cf. Figures 7 to 9).
The Cr-40Ni and Cr-30Ni alloys (Figure 7) both present significant amounts of chromium phase as well as of Ni-phase. Inside this nickel phase, some thin dark lamellae can be observed. These ones may result from a transformation in the solid state during cooling, due to the decrease in solubility of Cr in the nickel phase. These strips of chromium phase probably started growing from the neighbour of the existing areas of chromium phase and grew inward the nickel phase.

The reverse occurred inside the Cr-phase. Indeed, the solid state transformations induced the nucleation of Ni-phase inside the chromium matrix, the growth of which led to the little pale parts visible inside the matrix. This phenomenon is clearly visible in the Cr-30Ni alloy (Figure 7, bottom).

In the Cr-20Ni alloy, the aging for 50 hours at 1200°C obviously allowed chemical homogenization of the chromium phase (revealed by homogeneous grey colour), while the dendrite-like nickel based particles coarsened. This led to the areas of mixed nickel phase (containing 63 wt.%Cr) and chromium phase (containing about 19 wt.% Ni) visible in the aged Cr-20Ni alloy, dispersed in the chromium phase.

The aged Cr-10Ni alloy (Figure 9) contains two phases only: the first one in grey colour (Figure 9 bottom) is a chromium phase (containing about 60wt.% Cr) and is present inside the interdendritic spaces. The dark phase, which is the matrix of this alloy, is identified by EPMA (Electron Probe Micro-Analysis) as a chromium nitride which is imbricated with the chromium phase. These nitrides are identified by XRD as being Cr_2N.

In the case of the Cr alloy (Figure 10), some dark phases appeared inside the matrix. No other element was detected by WDS analysis, but chromium nitrides have appeared, as revealed by X-ray cartography.

3.4 Hardness evolution during aging

The hardness of the alloys was measured by Vickers indentation in their as-cast states and in the aged state. Data coming from [8], the hardness of Ni-xCr alloys (x=0 to 33 wt.%) elaborated following the same route as the present alloy, are added to extend the results to the binary chromium-containing nickel-based alloys.

The hardness of the alloys in their as-cast states (in blue colour in Figure 11) presents a bell shaped curve when plotted versus the chromium content. The Cr alloy is the one which has the lowest hardness (162 ± 2 Vickers). But when some nickel is added (2.5 to 10 wt.% Ni), the hardness increases strongly (up to 758 ± 20). The hardness still continues to increase with rising nickel addition until reaching 20wt.%Ni. The maximum hardness is obtained for the Cr-20Ni alloy (841 ± 0), the first alloy containing two phases in the as-cast state. When the level of nickel is further increased, the nickel phase is more present inside the alloys and the hardness decreases (722 ± 30 for the Cr-30Ni alloy, 446 ± 7 for the Cr-40Ni alloy and 220 ± 6 for the Cr-50Ni alloy).

The evolution of the hardness of the alloys after the aging treatment is dependent on the alloy composition (red coloured curve in Figure 11).

When the microstructure of the alloys showed no evolution during the aging treatment, the hardness remained the same. This is the case for the Cr-50Ni, Cr-40Ni and Cr alloys.

In contrast, the hardness of the Cr-30Ni and the Cr-20Ni alloys has significantly decreased from the as-cast state to the aged state. This is not necessarily in relation with the important change of microstructure observed after the aging treatment (appearance of lamellae of chromium phase inside the nickel one and the corresponding precipitation of nickel phase inside the chromium one (comparison of

Figures 7 and 8 with Figures 3 and 4). Indeed, these microstructure changes look like solid state transformation during the slow post-aging cooling (much slower than the post-solidification one). In the case of the Cr-10Ni alloy, a huge augmentation in hardness (from 758 ± 18 to 972 ± 59 Vickers) is noted between the as-cast state and the aged state. This augmentation is provoked by the presence of the Cr_2N phase.

3.5 Hardness in relation to phase fractions

The hardness of the as-cast single-phased Ni-based nickel-chromium alloys seemed to increase almost linearly with the Cr content [8]. A similar evolution of the hardness of the single-phased Cr-based chromium-nickel alloys with Ni content was noticed (but not linear). The evolution of hardness with composition of the double-phased Cr-Ni alloys was studied earlier on Ni-30Cr-xC alloys [9], Ni-30Cr-xC alloys [10] and Fe-30Cr-xC [11] alloys (x varying from 0 to 2%, all contents in weight percents) composed of a rather soft phase (the metallic matrix) and a much harder one (chromium carbides). Even if the hardness levels of the two phases present in the alloys studied here are not so different (soft Ni(Cr) phase and hard Cr(Ni) phase) two similar models of hardness evolution as presented in [9 to 11] were applied in this study. In the two following equations:

$$H_{alloy} = f_v(Cr) \times H(Cr) + f_v(Ni) \times H(Ni) \qquad \text{(Eq. 1)}$$

$$H_{alloy} = f_v(Cr) \times H'(Cr) + f_v(Ni) \times H(Ni) \qquad \text{(Eq. 2)}$$

$f_v(Cr)$ and $f_v(Ni)$ denote the volume fractions of the Cr phase and of the Ni phase, H(Cr) and H'(Cr) the hardness of the Cr phase for its Ni content, and H(Ni) the hardness of the Ni phase for its Cr content.

$f_v(Cr)$ and $f_v(Ni)$ are supposed to be close to the surface fractions of the Cr phase and of the Ni phase measured by image analysis. Indeed, by considering the general shapes of the two phases (globally compact areas joined to one another for each phase, no particular microstructure orientation) this correspondence may be rationally done, as earlier done in another context (metallic matrix with rater compact and not oriented carbides [12-15]). H(Ni) is calculated from the Cr content in the nickel phase according to equation (Eq. 3) issued from the regression line describing the linear hardness evolution versus the Cr content in the Ni phase (Fig. 12 A). Similarly H(Cr) is calculated according to the equation (Eq. 4) describing the locally linear evolution of

the hardness versus the Cr content in the chromium phase (Fig. 12 B) around 90 wt.%Cr. Since it seems that the hardness evolution of the chromium phase is not quite linear another equation was considered (Eq. 5), based on the observation that the hardness rather seems staying almost constant at 758 Hv under 90wt.%Cr, measured for the 88wt.%Cr content (EDS result) in the Cr-10Ni alloy.

$$H(Ni) = 2.55 \times wt.\%Cr + 65.77 \quad \text{(Eq. 3)}$$

$$H(Cr) = -22.42 \times wt.\%Cr + 2754 \quad \text{(Eq. 4)}$$

$$H'(Cr) = 758\ Hv \quad \text{(Eq. 5).}$$

H(Ni) was thus calculated from (Eq. 3) for percentages of Cr equal to 47.7 wt.%Cr (→ 188 Hv), 50.2 wt.%Cr (→ 194 Hv) and 66.2 wt.%Cr (→ 235 Hv) in the nickel phase of the Cr-50Ni (92vol.% of nickel-phase and 8vol.% of chromium-phase), Cr-40Ni (28 and 72 vol.%) and Cr-30Ni (5 and 95 vol.%). The same law was applied for the aged double-phased alloys. For them, with wt.%Cr in nickel phase globally constant at a value of 55 wt.%, a constant hardness of 206Hv was considered, this time for the four double-phased alloys Cr-xNi with x varying from 50 to 20 wt.% since the chromium phase of the Cr-20Ni alloy was obviously homogenized during the 1200°C aging.

H(Cr) was calculated from (Eq. 4) for percentages of Cr equal to 69.5 wt.% (→ 1196 Hv), 65.1 wt.% (→ 1294 Hv) and 77.6 wt.%Cr (→ 1014 Hv) in the chromium phase of the Cr-50Ni, Cr-40Ni and Cr-30Ni. H(Cr) was recalculated from (Eq. 5) by supposing that the hardness of the chromium phase remained close to the final value of 758Hv (obtained for the Ni-richest single-phased Cr-10Ni alloy). Eq. 5 was applied for the aged double-phased alloys, too. For them, with wt.%Ni in chromium phase globally constant at the 21 wt.% value, a constant hardness of 758Hv was considered, for the four double-phased Cr-xNi alloys with x varying from 50 to 20 wt.%.

The experimental hardness values are plotted in Fig. 12 C for the as-cast alloys and in Fig. 13 for the aged Cr-50Ni (90vol.% of nickel-phase and 10vol.% of chromium-phase), Cr-40Ni (48 and 52 vol.%), Cr-30Ni (28 and 72 vol.%) and Cr-20Ni (3 and 97 vol.%) alloys, together with the model curves corresponding to (Eq. 1-2). For the as-cast state (Fig. 12 C) the three points logically correspond to each single-phased alloy. For the as-cast double-phased alloys, the model curve calculated from (Eq. 1) is rather far from the experimental results. The calculation from (Eq. 2) is more consistent. The variation curve of the hardness versus the Cr content clearly presents a negative

curvature, with a maximum value corresponding to the transition from the double-phased alloys to the the Ni-richest single-phased Cr-based alloy.

Because of better accuracy (Eq. 2) and (Eq. 5) were considered for the comparison of experimental hardness of the aged alloys and the model curve (Fig. 13). The two hardness values, measured and calculated, are rather consistent for the four aged (but not nitrided) double-phased alloys.

4. Discussion

One phase (for the Cr alloy and the Cr-10Ni one) or two phases were observed: a Cr-based Ni-containing BCC one and a Ni-based Cr-containing FCC one. In most of the double-phased alloys the two phases are imbricated and led to globally homogeneous alloys, showing good microstructure (by regards to what can be expected for the mechanical properties) and homogeneous chemical composition at the ingot scale. In contrast, all the alloys were sensitive to the rather fast cooling rate applied during solidification and solid state cooling. Indeed, according to the Cr-Ni binary diagram, the phases based on chromium have solidified first, except in the case of the Cr-50Ni. But severe chemical segregation during solidification (e.g. of Ni in the periphery of the chromium-phase grains in the Cr-20Ni and Cr-10Ni alloys) and metastable states (e.g. no Ni-phase precipitation inside the chromium phase and no Cr-phase precipitation in the nickel-phase for the Cr-40Ni and Cr-30Ni alloys) were revealed during the metallographic characterization of the as-cast alloys.

As showed by the examination of the aged alloys, they are isothermally exposed during time long enough at a temperature high enough and they are thereafter cooled at a rather slow cooling rate to present microstructure changes. First, the chemical homogenization of the phases was realized in the whole alloys (accompanied by a usual general microstructure coarsening in the double-phased alloys). The decrease in solubility of Ni in the chromium phase and of Cr in the nickel phase during cooling led to the solid state growth of each phase inside the other phase, with a classical lamellae feature (as pearlite in carbon steels) or another morphology. The part of structure changes to attribute to the isothermal aging, and the one to attribute to precipitation during the slow cooling of lamellar second phase in oversaturated phase areas, may be further confirmed by new experiments ended by fast cooling and even quenching instead slow cooling.

The surface fractions were significantly changed in some of the double-phased alloys during the aging treatment (more chromium phase and less nickel phase), simultaneously with the average contents in Ni in the first one and in Cr in the second one. The decrease in hardness, promoted by these surface fraction changes, seems predominant on the hardness variations resulting from the Ni and Cr contents in these chromium and nickel phases. Indeed, it was first found that the hardness of the aged alloys was lower than the as-cast ones, and second that the model hardness calculated from Eq. 2 fits the experimental curve for the as-cast alloys as well as for the aged alloys. It should be kept in mind that the microstructure coarsening may also have an effect on hardness.

The Cr-30Ni and Cr-20Ni alloys present the more promising microstructures for high mechanical properties at elevated temperature. This is suggested by their high room temperature hardness which is lowered by several tens of hours of exposure at high temperature, but nevertheless maintained at a high level. After aging treatment it is the Cr-10Ni which appeared as the hardest alloy, but this is due to the extended nitridation which converted most of the alloy into CrN or Cr_2N (hardness of 1093 and 1571 Hv5g [12], respectively). This phenomenon, which favours high brittleness for the Cr-10Ni alloy, was here seen also for pure chromium (the “Cr alloy”), but it did not occur in the other alloys. The double-phased imbricated microstructures of the Cr-20Ni and Cr-30Ni alloys, probably lead to a protection of the BCC chromium phase by the compact FCC nickel phase, against fast inwards diffusion of nitrogen.

5. Conclusions

Thus, these refractory alloys can be elaborated and shaped by casting, at least as small pieces. After their characterization in the as-cast state and after high temperature exposure, it was found that some potentially interesting imbricated microstructures of Cr-rich BCC phase (favouring oxidation resistance) and FCC phase (favouring mechanical strength) may be obtained in this system. The not monotonous hardness evolution with the Cr content and its decrease with the aged state were explained by the fact that it results from the superposition of the hardness increase of the nickel phase with its Cr content, the hardness increase of the chromium phase with its Ni content and the volume proportions of chromium phase and nickel phase. In consequence, there is a maximum hardness value near the Cr-30Ni and Cr-20Ni alloys, in the as-cast state as well as in the aged state, designating that such alloys

may be, after optimization, an alloys' base very resistant to mechanical stresses at high temperature as well as to hot oxidation and corrosion (great Cr reservoirs) and not so threatened by nitridation as the Cr-richest alloys of this study.

Future work will be the characterization of these high temperature properties, mechanical and chemical, followed by the development, from these bases, of optimized and thus probably more complex alloys. Special attention will be given to the possible too low fracture toughness suggested by the very high values of hardness observed for some of the alloys. Among the new elements to add to these Cr-Ni bases, some elements well known for their beneficial effect on fracture toughness will be considered and tested.

6. Acknowledgements

The authors wish to thank P. Villeger for the X-Ray Diffraction runs.

7. References

[1] Sims, C.H.W. (1972) The superalloys, New York: John Willey

[2] Bradley, E.F. (1988) Superalloys: A Technical Guide, ASM International, Metals Park.

[3] Kofstad, P. (1988) High Temperature Corrosion, Elsevier Applied Science, London.

[4] Defrance, A. Metallurgie du Chrome. Techniques de l'Ingénieur, **2245** 1-10 (1988).

[5] Lide, D.R. (2009) CRC Handbook of Chemistry and Physics, ed 90, CRC Press Inc.

[6] Thermo-Calc N version: Fondation for Computational Thermodynamics, Stockholm, Sweden, Copyright (1993,2000).

[7] STGE: Scientific Group Thermodata Europe database, update 1992.

[8] Berthod, P, Conrath, E., Influence of the chromium content on the hardness of Co-based, Ni-based and Fe-based chromium-containing binary alloys. Materials Science: An Indian Journal, in press.

[9] Berthod, P. Room temperature hardness of carbides-strengthened cast alloys in relation with their carbon content and aging temperature. Part I: Case of nickel alloys. Materials Science and Technology, **25(5)**, 657-662 (2009).

[10] Berthod, P. Room temperature hardness of carbides-strengthened cast alloys in relation with their carbon content and aging temperature. Part II: Case of cobalt alloys. Materials Science and Technology, **25(5)**, 663-669 (2009).

[11] Berthod, P. Room temperature hardness of carbides-strengthened cast alloys in relation with their carbon content and aging temperature. Part II: Case of iron alloys. Materials Science and Technology, **25(8)**, 1003-1008 (2009).

[12] Berthod, P., Michon, S., Aranda, L., Mathieu, S., Gachon, J.-C. Experimental and thermodynamic study of the microstructure evolution in cobalt-base superalloys at high temperature. Calphad, **27(4)**, 353-359 (2003).

[13] Berthod, P., Aranda, L., Vébert, C., Michon, S. Experimental and Thermodynamic Study of the Microstructural State at High Temperature of Nickel base Alloys containing Tantalum. Calphad, **28(2)**, 159-166 (2004).

[14] Berthod, P., Hamini, Y., Héricher, L., Aranda, L. Experimental and thermodynamic study of tantalum-containing iron-based alloys reinforced by carbides: Part I-Case of (Fe, Cr)-based ferritic steels. Calphad, **31(3)**, 351-360 (2007).

[15] Berthod, P., Lemoine, P., Aranda, L. Experimental and thermodynamic study of nickel-based alloys containing chromium carbides: Part I – Study of the Ni-30wt%Cr-xC system over the [0 - 2.0wt%C] range. Calphad, **32(3)**, 485-491 (2008).

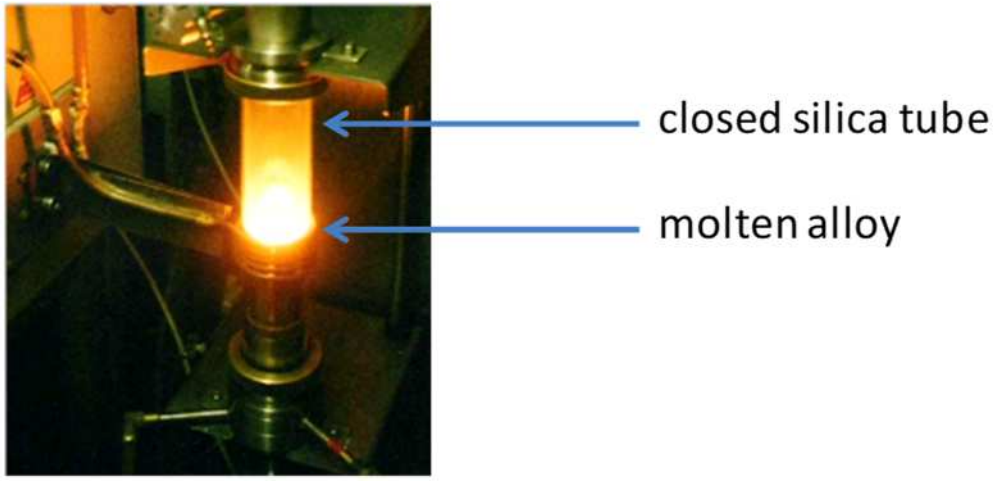

Fig. 1. Fusion of an alloy in the high frequency induction furnace (CELES)

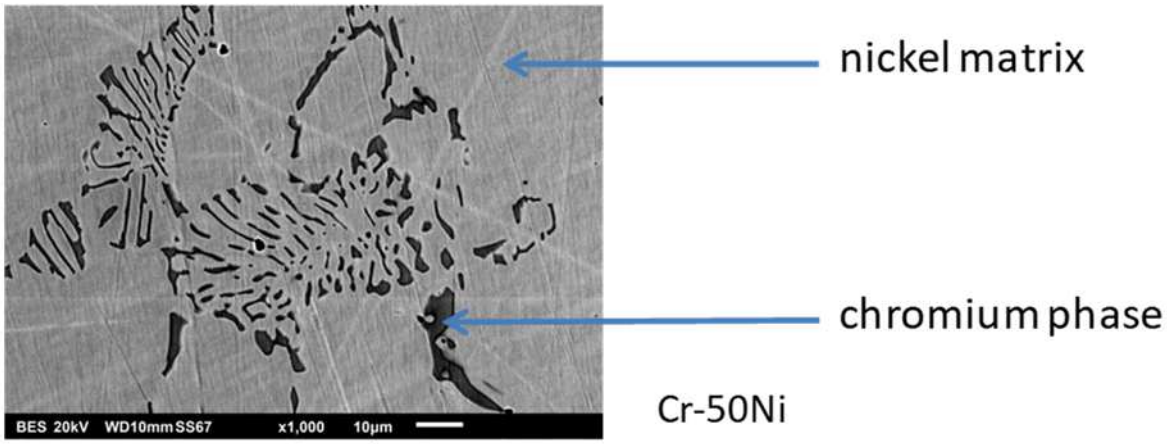

Fig. 2. As-cast microstructures of the Cr-50Ni alloy

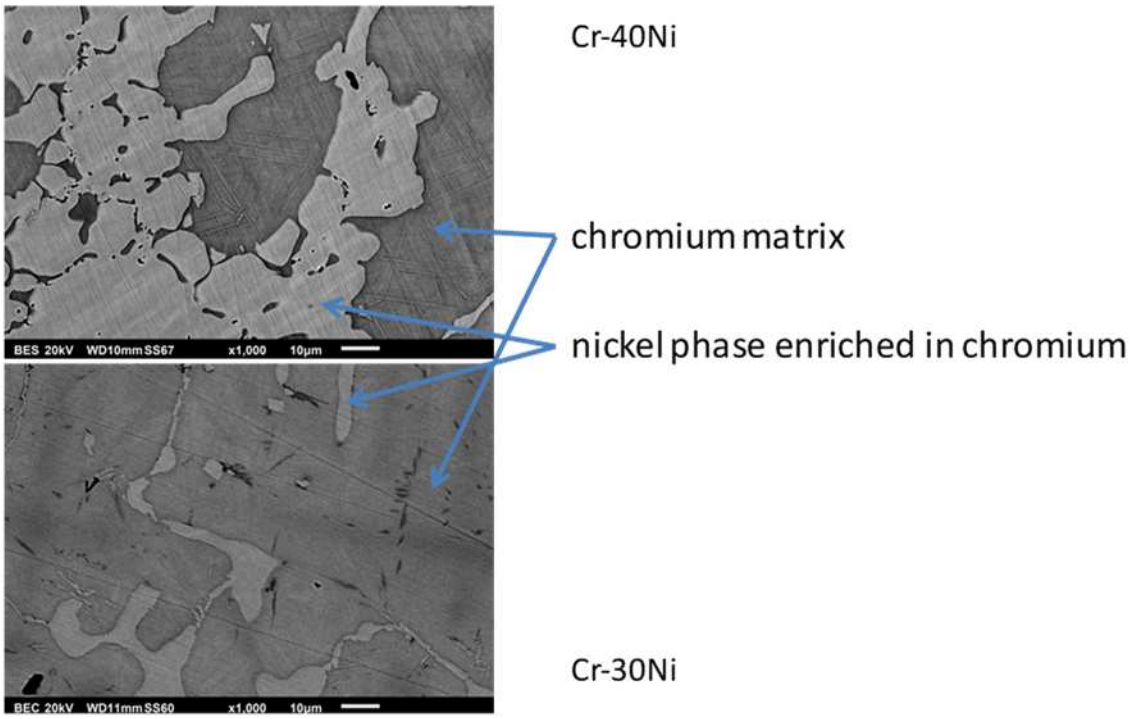

Fig. 3. As-cast microstructures of the Cr-40Ni and the Cr-30 Ni alloys

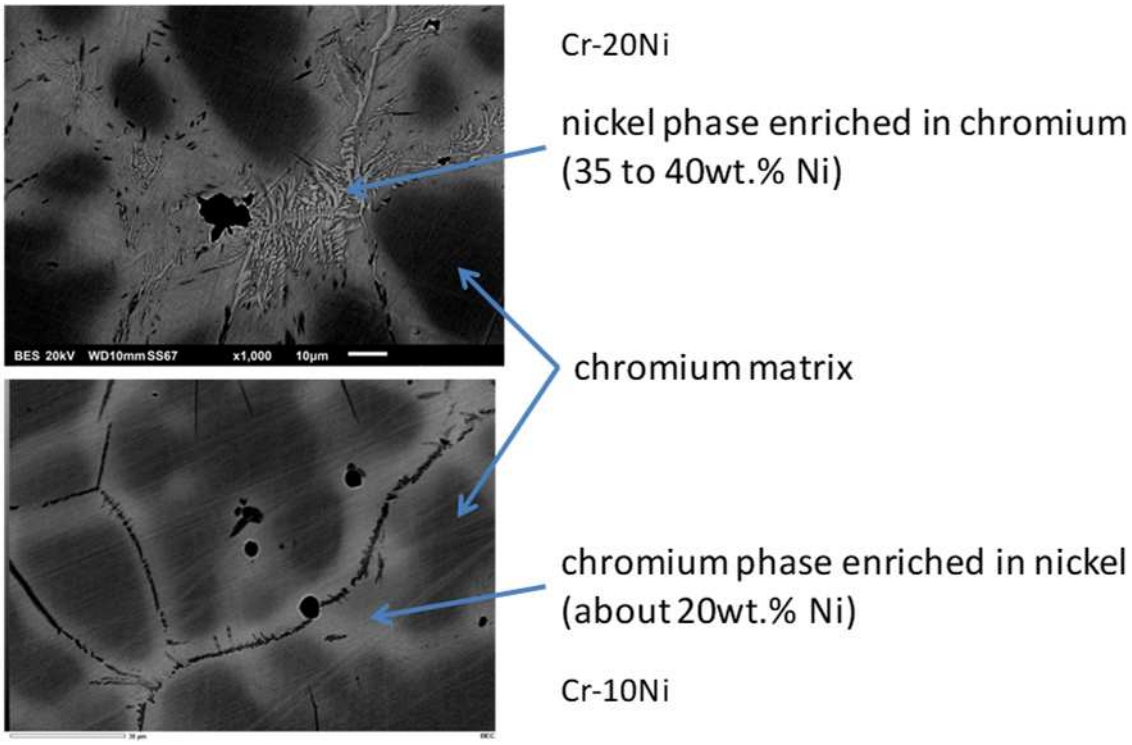

Fig. 4. As-cast microstructures of the Cr-20Ni and the Cr-10 Ni alloys

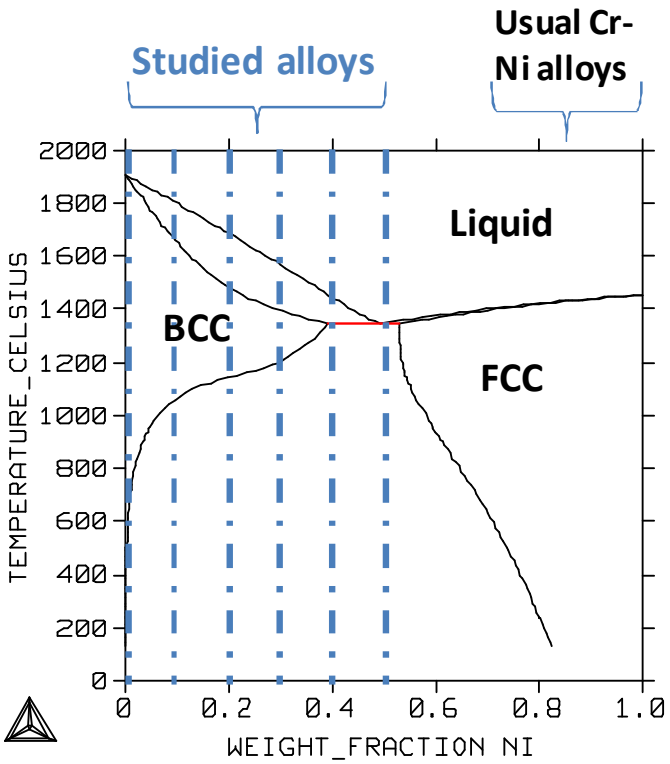

Fig. 5. Cr-Ni binary diagram computed by using the Thermo-Calc software

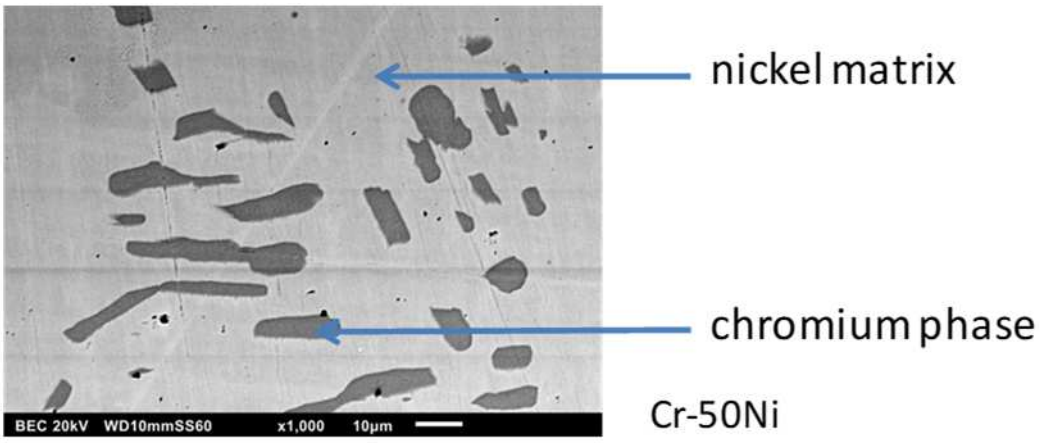

Fig. 6. Microstructure of the Cr-50Ni alloy after high temperature exposure (1200°C, 50h)

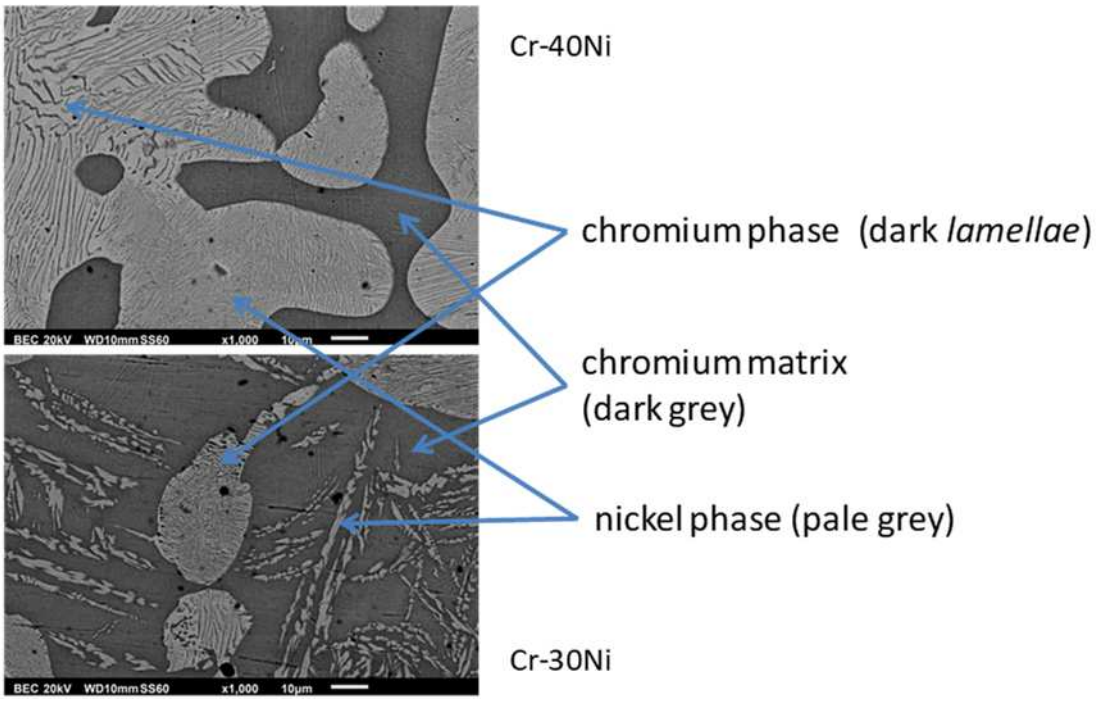

Fig. 7. Microstructures of the Cr-40Ni and Cr-30Ni alloys after high temperature exposure (1200°C, 50h)

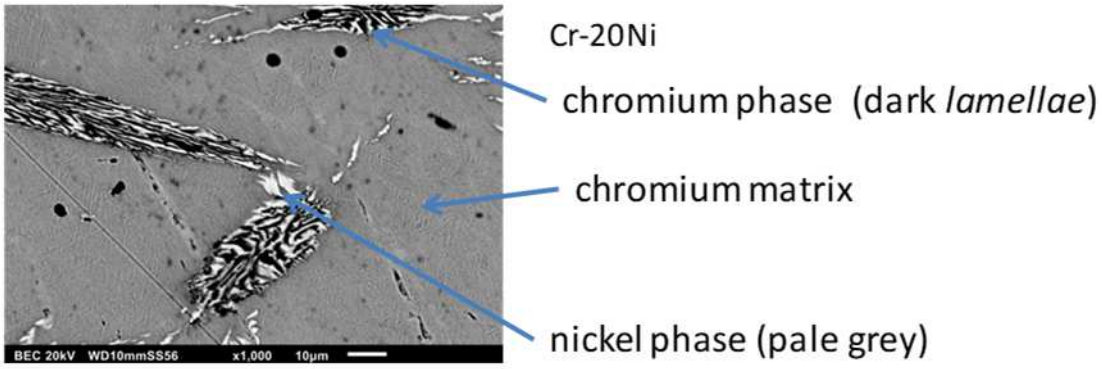

Fig. 8. Microstructure of the Cr-20Ni after high temperature exposure (1200°C, 50h)

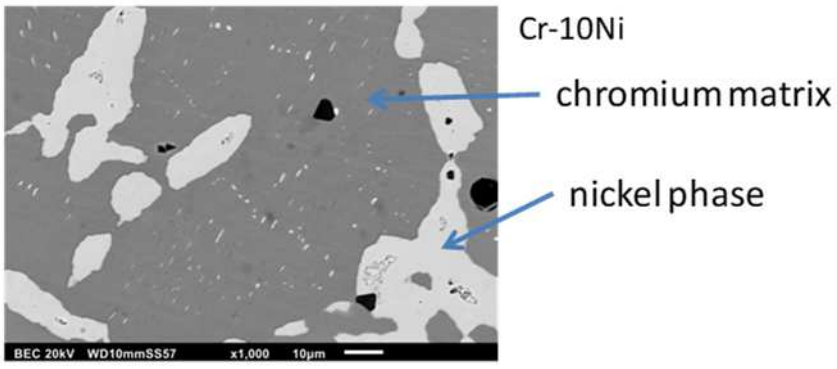

Fig. 9. Microstructures of the Cr-10Ni after high temperature exposure (1200°C, 50h)

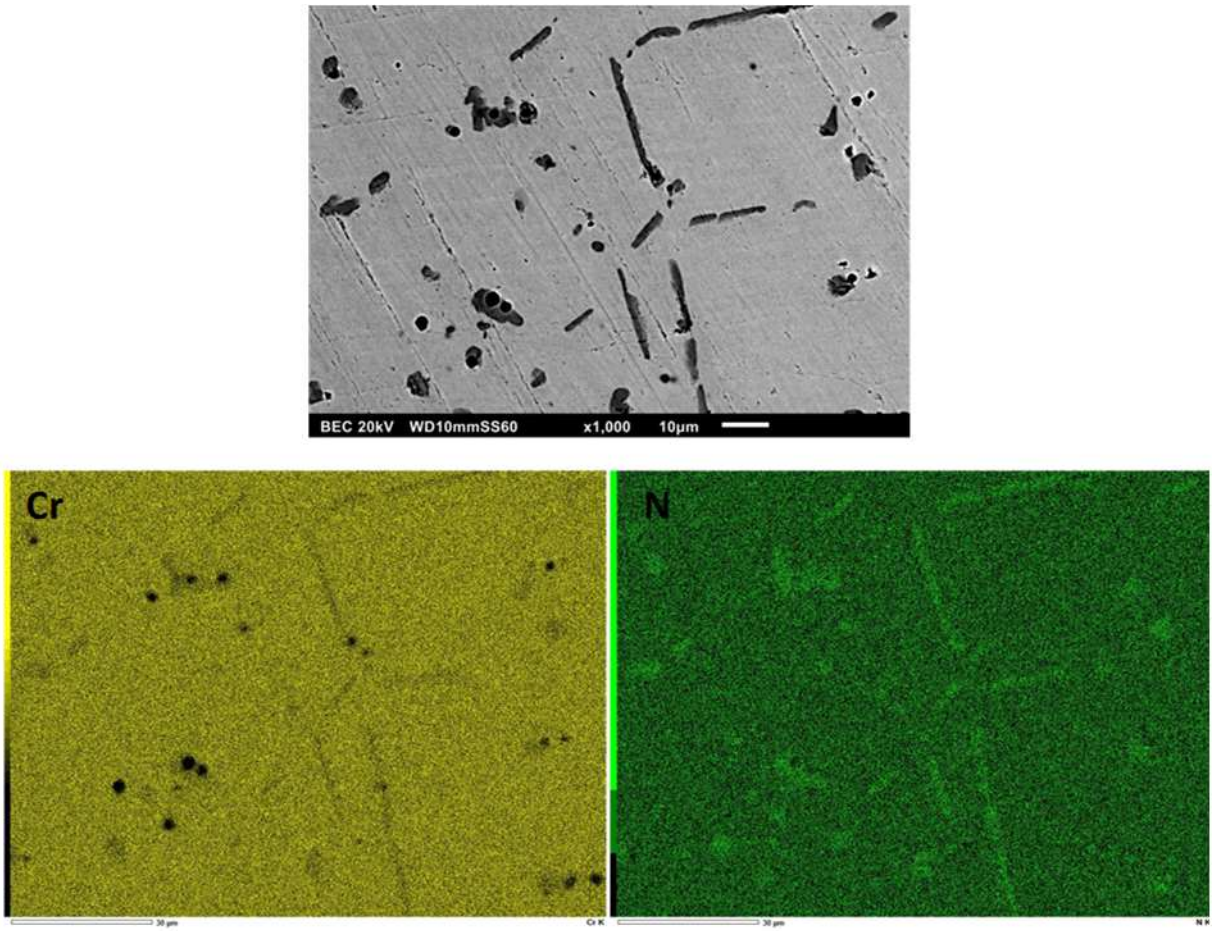

Fig. 10. Microstructures of the Cr alloy after high temperature exposure (1200°C, 50h) and X-Ray cartography

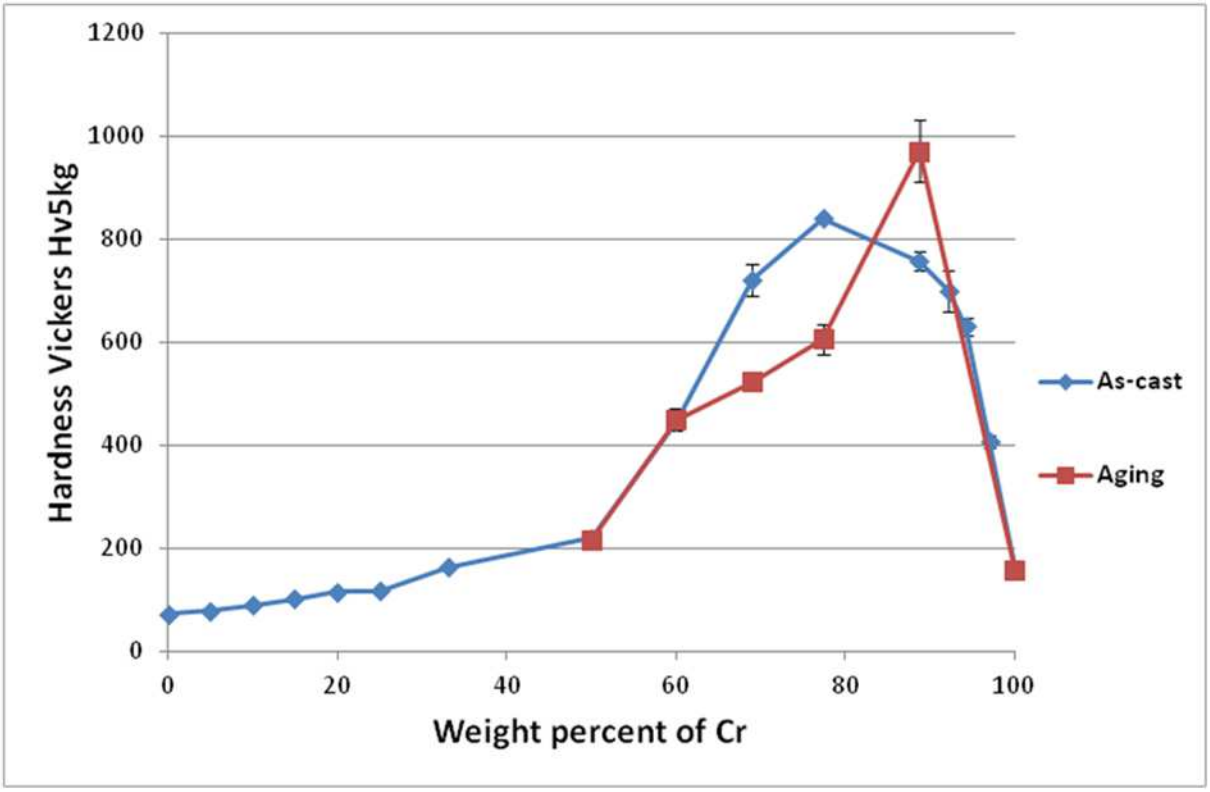

Fig. 11. Hardness as-cast and after high temperature exposure (1200°C, 50h) of the alloys under 5 kilograms

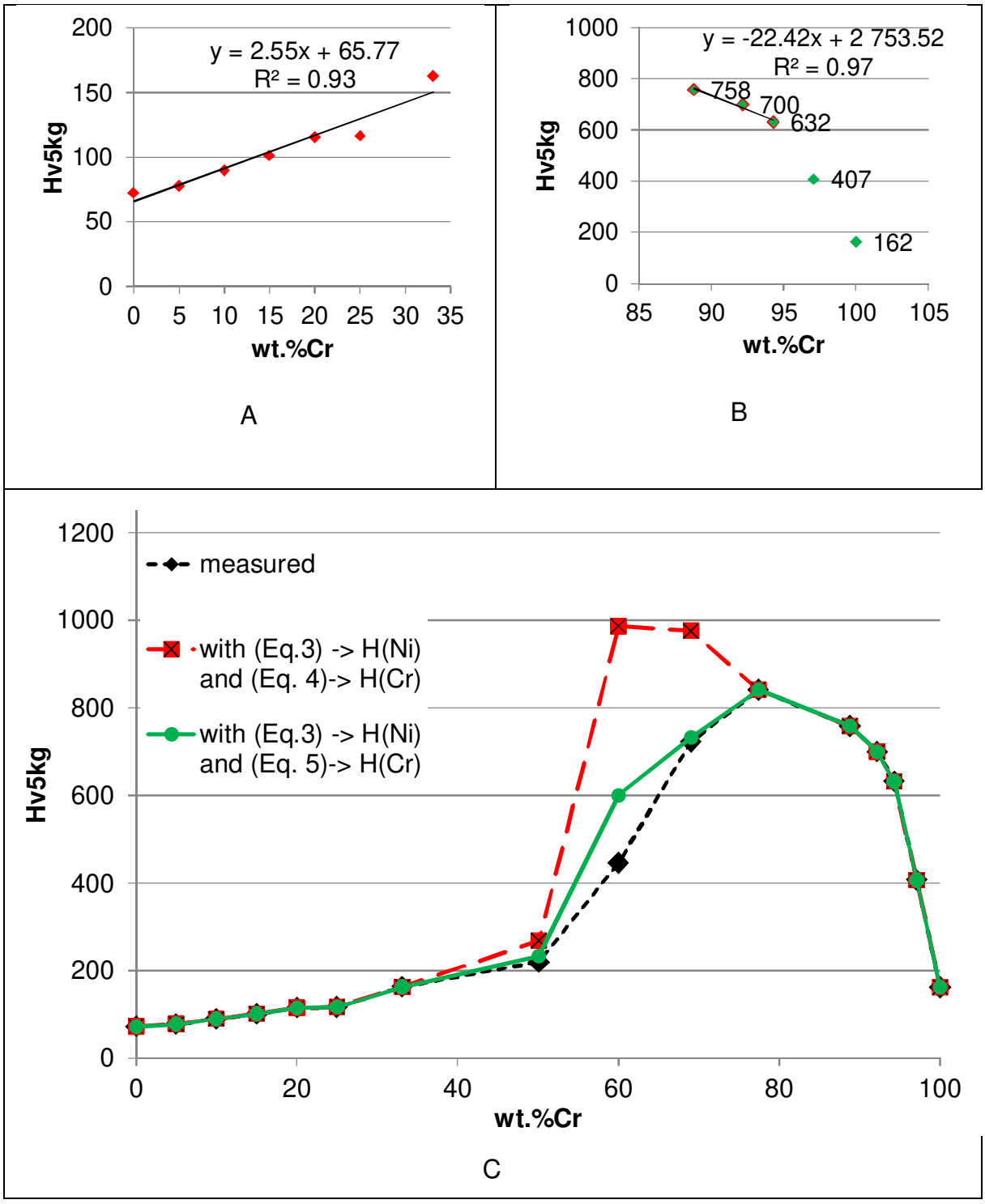

Fig. 12. Comparison of the measured hardness of the as-cast alloys with the theoretical values issued from equation 1 (“slopes in A and B”) and from equation 2 (“slope in A and 758Hv in B”)

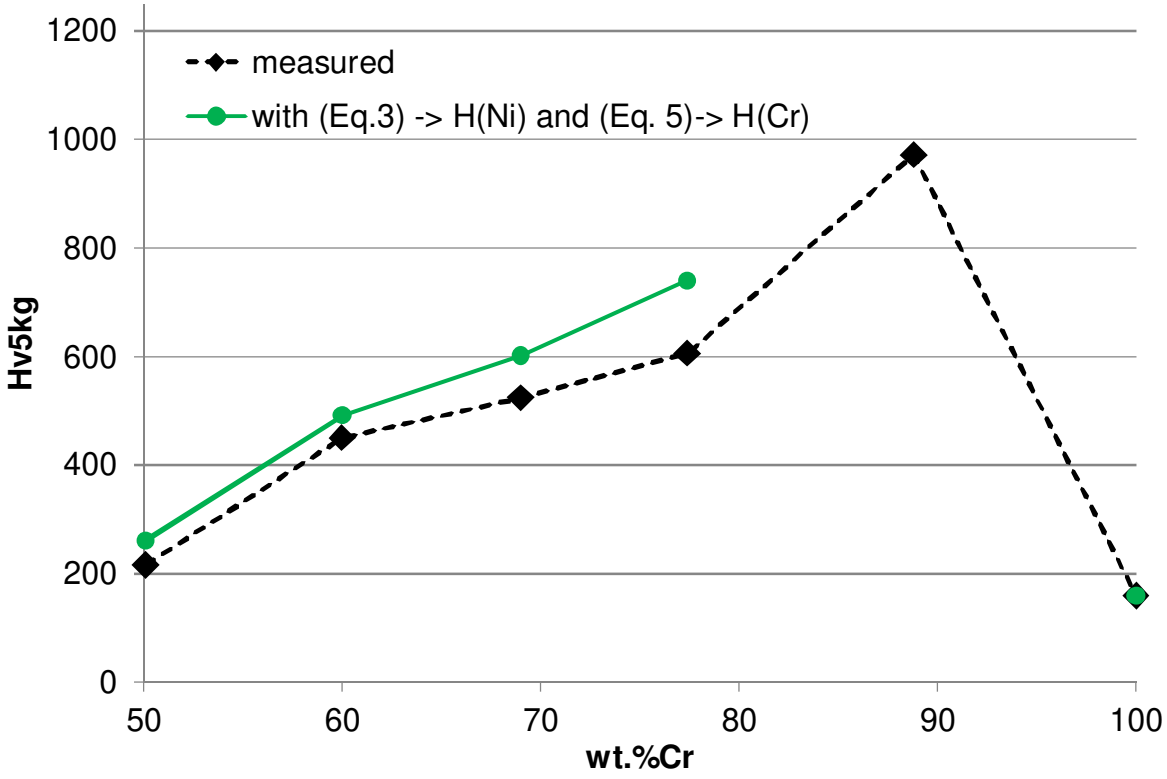

Fig. 13. Comparison of the measured hardness of the aged alloys with the theoretical values issued from equation 2 (“slope in A and 758Hv in B”)

Tab. 1. Names and targeted compositions of the binary alloys (in weight percent)

Name of the alloys	Targeted composition (in wt.%)	
	Cr	Ni
Cr-50Ni	balance	50
Cr-40Ni		40
Cr-30Ni		30
Cr-20Ni		20
Cr-10Ni		10
Cr-7.5Ni		7.5
Cr-5Ni		5
Cr-2.5Ni		2.5
Cr		0

Tab. 2. Chemical compositions of the alloys measured by EDS analysis

Name of the alloy	wt.% measured by SEM (5 zones)	
	Cr	Ni
Cr-50Ni	50.1±0.4	49.9±0.4
Cr-40Ni	60.0±0.6	40.0±0.6
Cr-30Ni	69.0±0.3	31.0±0.3
Cr-20Ni	77.4±0.9	22.6±0.9
Cr-10Ni	88.8±0.4	11.2±0.4
Cr-7.5Ni	92.2±0.5	7.8±0.5
Cr-5Ni	94.3±0.1	5.8±0.1
Cr-2.5Ni	97.1±0.3	2.9±0.3
Cr	No impurities	

Tab. 3: Surface analysis of the two phases in the as-cast Cr-50Ni alloy (Photoshop Software)

	Cr phase Cr (%)	Ni phase Ni (%)
Cr-50Ni as-cast	13.9 ± 2.7	86.1 ± 2.7